A Three-Port Three-Phase DC-DC Converter for Hybrid Low Voltage Fuel Cell and Ultracapacitor

Danwei Liu
Dept. of ECE
FAMU-FSU College of Engineering
Tallahassee, FL, 32310, USA
liu@caps.fsu.edu

Hui Li
Dept. of ECE
FAMU-FSU College of Engineering
Tallahassee, FL, 32310, USA
hli@caps.fsu.edu

***Abstract* – A novel three-port three-phase dc-dc converter is proposed in this paper to interface with low voltage fuel cell and ultracapacitor (UC). Major features of the converter include: 1) provide an integrated energy conversion solution with combined power flow from fuel cell and UC; 2) draws and injects smooth current from the fuel cell and UC; 3) increase input current rating by interleaving three phases, not by paralleling components; 4) reduce core number and current ripple with improved efficiency by integrating three input inductors into a single core with coupling; 5) achieve zero-voltage-switching (ZVS) over a wide range by hybrid pulse-width-modulation (PWM) and phase-shift-modulation (PSM) control. This converter has a great potential application in fuel cell vehicle and distributed power generation. The operation principle, steady state analysis and integrated magnetic design are presented in the paper. Circuit simulation results are provided to verify the theoretical analysis.**

I. INTRODUCTION

Fuel cells are considered to be one of the most promising power generation devices because of their environmentally friendly energy conversion. Fuel cells have a slow response due to the natural electrochemical reactions required for the balance of enthalpy. Therefore bidirectional energy storage is required as an external levelling system to sink/source the power difference. A multi-port dc-dc converter, one of which is bidirectional, is promising in terms of cost, power density, efficiency and simplicity.

Since each cell in a fuel cell stack has a low output voltage (0.6 V at full load), it is necessary to stack many cells in series to obtain a reasonable output voltage. Stacking many cells in series adds to the complexity of the system including a complicated plumbing to uniformly distribute the fuel and difficult water/thermal management. Due to these limitations, a lower output voltage fuel cell is preferred. For an example, fuel cell with 22 V nominal output voltage was adopted for 2003 International Future Energy Challenge sponsored by Department of Energy, USA.

An ultracapacitor (UC) has an advantage over batteries in terms of transient energy storage. It has other advantage that it can be recharged and charged virtually an unlimited number of times and thus much less maintenance is required. The SOC of UC is a simple function of voltage so a sophisticated indictor is not required. The UC supports very low voltages (1-2.5V). A stack of series-connected UCs is required to hold up tens of Volts. Stacking many cells in series to support higher voltage requires extra dc voltage balance control that results in the adding cost and complexity. The lower output voltage UC is thereby also preferred in the application.

The low output voltage of fuel cell and UC making the design of multi-port dc-dc converter very challenging. For example, an isolated dc/dc converter is needed to convert low voltage dc to a dc voltage higher than 400 V for a 240 V ac output at 5 kW continuous and 10 kW peak. This dc/dc converter will see high current at both fuel cell and UC side. Although the power from fuel cell is unidirectional, a bidirectional power flow is required between UC and the load. In addition, UC has a widely changing dc operating voltage that may affect the converter operation. Most of current bidirectional multi-port dc-dc converter deals with the low output power and/or low input current applications [1-4]. This paper proposed a three-port three-phase dc-dc converter to address the above design issues. Major features of the converter include: 1) provide an integrated energy conversion solution with combined power flow from fuel cell and UC; 2) draws and injects smooth current from the fuel cell and UC; 3) increase input current rating by interleaving three phases, not by paralleling components; 4) reduce core number and current ripple with improved efficiency by integrating three input inductors into a single core with coupling; 5) achieve zero-voltage-switching (ZVS) over a wide range by hybrid pulse-width-modulation (PWM) and phase-shift-modulation (PSM) control. This converter has a great potential for application where an interface between low voltage fuel cells, low voltage energy storage element and high voltage dc bus is required. Examples include distributed power generation systems and fuel cell vehicle.

The paper is organized as follows. Section II gives a brief introduction of the proposed converter. In section III an integrated three-phase coupling inductors was proposed and analyzed by using equivalent circuit model. In section IV, the operation principle of proposed converter was presented and simulation results was provided. This topology was also compared with single-phase version in terms of power device stress, transformer utilization and capacitor specification.

II. PROPOSED THREE- PHASE DC-DC CONVERTER

Fig. 1 shows the proposed converter circuit. It consists of two input power stages and an output power stage. Port I is a three-phase boost converter connected with fuel cell to boost the low fuel cell voltage to a higher value by controlling the duty cycle of switching devices S_a, S_b and S_c. The diodes D_a, D_b and D_c prevent reverse power flow into the fuel cell.

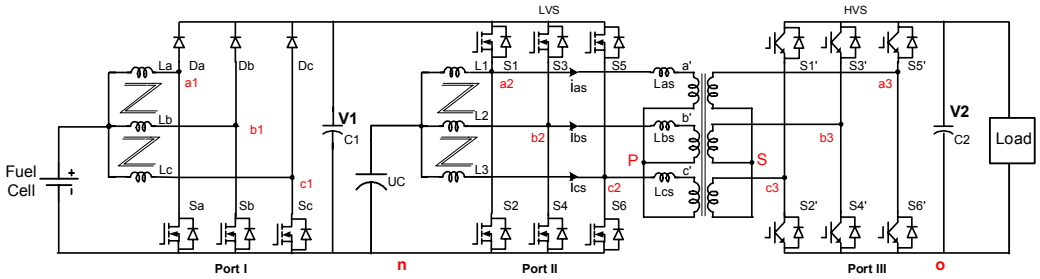

Fig. 1 Proposed three-port three-phase current source ZVS bidirectional dc-dc converter for fuel cell and UC

The converter is designed to operate at critical conduction mode (CRM) to eliminate reverse-recovery of diodes. Although the current ripple in each phase is large, the combined current seen by fuel cell is continuous and smooth. Port II (UC) and III (load) forms a three-phase dual active bridge current source ZVS bidirectional dc-dc converter (TPDAB). The power flow is controlled by the phase shift between active bridges at low voltage side (LVS) and high voltage side (HVS). The leakage inductance of high frequency transformer is acting as intermediate element to store and transfer the power. As long as the dc voltage across LVS and HVS is kept equal, both rms current and peak current of switches and transformer of TPDAB are minimized as well as the ZVS soft switching of TPDAB could be maintained. However, the variation of operating voltage of UC is usually within 50% ~ 100%. Combining varied duty cycle and phase shift modulation can compensate this variation.

The unidirectional boost converter and bidirectional TPDAB converter are integrated by sharing a common low voltage dc bus with a dc capacitor C_1. The capacitor should be able to handle high switching current ripple and maintain a nearly constant dc bus voltage. On the other hand, the input inductor current ripple of L_a ~ L_c, L_1~L_3 should be kept low to reduce core loss and, more importantly, to provide a favourable operation condition for fuel cells and UC. The converter works in an interleaving manner and each phase output is 120° apart from each other. In this mode, the ripple frequency will be increased to three times the switching frequency and current ripple will be greatly reduced due to cancelling effects between each phase.

II. TRREE PHASE COUPLING INDUCTORS WITH INTEGRATED MAGNETICS

One challenge for three-phase converter is the practical realization of a three-phase inductor with identical inductance. There are two three-phase inductors L_a ~ L_c and L_1~L_3 in the proposed converter. An integrated magnetic core is utilized for each inductor. Fig. 2 shows how the magnetic structure of coupling inductors is obtained. One thing should be noted is that the core with EI shape is used to build three-phase inductors, which is a standard core shape and easier to built comparing with other custom designed three-phase core [8].

Fig. 2 (a) represents a traditional configuration with independent core structure for each individual inductor,

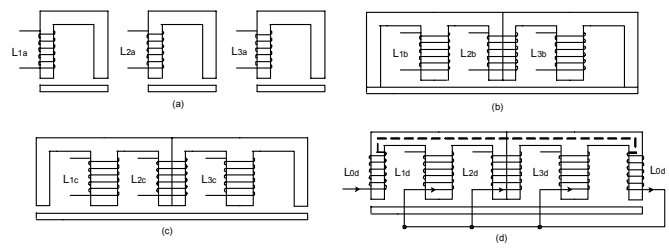

Fig. 2 Core structures and corresponding equivalent circuits

where three cores are used independently.

The three inductors could also be integrated as shown in Fig. 2(b). The three inductors are decoupled the core loss of the outer leg is reduced and magnetic efficiency can be improved. However, the ripple current in each inductor and flux ripple in the centre leg remains the same as that in a single-phase inductor. Furthermore, the core shown here is not a standard industry practice. The air gap of the core need to be precisely adjusted and filling need to be added to ensure mechanical stability [6].

The coupling effect of three inductors could be realized by the core structure as shown in Fig. 2(c). In this structure, the current and flux ripple of each centre leg could be reduced comparing with the structure of Fig. 2(b).

Fig 2(d) shows the proposed structure with another two identical windings on the outer legs and connected in parallel. In this arrangement, with the same overall physical inductances, the minimum phase current ripple could be achieved. In addition, the two additional windings inversely coupled with the centre windings and will help to cancel the flux ripple in the outer legs. Therefore, the core loss could be further reduced.

The three inductors in Fig, 2(d) could not be treated as independent inductors because coupling effects. In order to get the equivalent circuit model of the three-phase inductors, the magnetic model of the proposed magnetic structure should be derived first. The proposed integrated magnetic structure and corresponding gyrator model [10] are shown in Fig. 3 (a) and (b) respectively. Here, $\Re_0$ -$\Re_3$ are the magnetic reluctances of outer leg and three centre legs respectively with air gaps considered and $\Re_t$ is the magnetic reluctance of the core between two legs. In the gyrator model, C_0~C_3 and C_t represent the corresponding reluctances respectively. The currents $i_{c0}(s)$ ~ $i_{c4}(s)$ represent the $d\phi/dt$ of the corresponding core legs. In order to simplify the analysis, the reluctance $\Re_t$ and corresponding C_t in the gyrator model are ignored because of its short magnetic path and low reluctance.

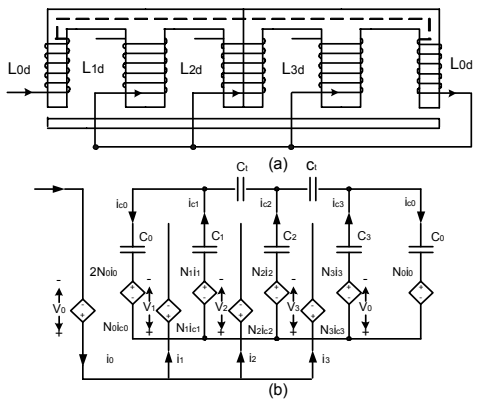

Fig. 3 (a) Proposed core structure; (b) corresponding gyrator model

Based on gyrator model in Fig. 3(b), the expressions for $i_{c0}(s)$, $i_{c1}(s)$, $i_{c2}(s)$ and $i_{c4}(s)$ could be found as follows:

$$i_{c1}(s) = N_1 i_1(s)\cdot\frac{C_1(2C_0+C_2+C_3)}{2C_0+C_1+C_2+C_3}\cdot s - N_2 i_2(s)\cdot\frac{C_1C_2}{2C_0+C_1+C_2+C_3}\cdot s - N_3 i_3(s)\cdot\frac{C_1C_3}{2C_0+C_1+C_2+C_3}\cdot s - 2N_0 i_0(s)\cdot\frac{C_1C_0}{2C_0+C_1+C_2+C_3}\cdot s \quad (1)$$

$$i_{c2}(s) = N_2 i_2(s)\cdot\frac{C_2(2C_0+C_1+C_3)}{2C_0+C_1+C_2+C_3}\cdot s - N_1 i_1(s)\cdot\frac{C_1C_2}{2C_0+C_1+C_2+C_3}\cdot s - N_3 i_3(s)\cdot\frac{C_2C_3}{2C_0+C_1+C_2+C_3}\cdot s - 2N_0 i_0(s)\cdot\frac{C_0C_2}{2C_0+C_1+C_2+C_3}\cdot s \quad (2)$$

$$i_{c3}(s) = N_3 i_3(s)\cdot\frac{C_3(2C_0+C_1+C_2)}{2C_0+C_1+C_2+C_3}\cdot s - N_2 i_2(s)\cdot\frac{C_2C_3}{2C_0+C_1+C_2+C_3}\cdot s - N_1 i_1(s)\cdot\frac{C_1C_3}{2C_0+C_1+C_2+C_3}\cdot s - 2N_0 i_0(s)\cdot\frac{C_3C_0}{2C_0+C_1+C_2+C_3}\cdot s \quad (3)$$

$$i_{c0}(s) = N_0 i_0(s)\cdot\frac{C_0(C_0+C_2+C_3)}{2C_0+C_1+C_2+C_3}\cdot s - N_1 i_1(s)\cdot\frac{C_0C_1}{2C_0+C_1+C_2+C_3}\cdot s - N_2 i_2(s)\cdot\frac{C_0C_2}{2C_0+C_1+C_2+C_3}\cdot s - N_3 i_3(s)\cdot\frac{C_0C_3}{2C_0+C_1+C_2+C_3}\cdot s \quad (4)$$

The voltages of the inductor are:

$$v_1(s) = N_1 i_{c1}(s),\ v_2(s) = N_2 i_{c2}(s),\ v_3(s) = N_3 i_{c3}(s),\ v_0(s) = N_0 i_{c0}(s) \quad (5)$$

Substituting (1)~(4) into equation (5) and considering $i_0(s) = i_1(s) + i_2(s) + i_3(s)$, we have

$$v_1(s) = (L_d + M_0)i_1(s)\cdot s + (M_1 + M_0)i_2(s)\cdot s + (M_1 + M_0)i_3(s)\cdot s \quad (6)$$

$$v_2(s) = (M_1 + M_0)i_1(s)\cdot s + (L_d + M_0)i_2(s)\cdot s + (M_1 + M_0)i_3(s)\cdot s \quad (7)$$

$$v_3(s) = (M_1 + M_0)i_1(s)\cdot s + (M_1 + M_0)i_2(s)\cdot s + (L_d + M_0)i_3(s)\cdot s \quad (8)$$

$$v_0(s) = (L_0 + M_0)i_0(s)\cdot s \quad (9)$$

Assuming the air gap thicknesses of the three centre legs are the same, so $C_1 = C_2 = C_3 = C$. Assuming $N_1 = N_2 = N_3 = N$, $\alpha = \frac{C_0}{C}$, and $\beta = \frac{N_0}{C}$, we have,

$$L_0 = \beta^2 N^2 C\cdot\frac{6\alpha}{3+2\alpha} \quad (10)$$

$$L_d = N^2 C\cdot\frac{2+2\alpha}{3+2\alpha} \quad (11)$$

$$M_0 = -2\beta N^2 C\cdot\frac{\alpha}{3+2\alpha} \quad (12)$$

$$M_1 = -N^2 C\cdot\frac{1}{3+2\alpha} \quad (13)$$

Where L_d is the self-inductance of three windings on the centre legs, L_0 is the self-inductance of the two windings on the outer legs, M_0 is the mutual inductance between three centre leg windings and outer leg windings, M_1 is the mutual inductance between three outer leg windings.

The equations (6)~(9) could be represented by the equivalent circuit. The equivalent circuit can be simplified considering that the inductor L_0 is decoupled with L_d and the inductor $L_0 + M_0$ can be integrated into the rest three inductors.

The inductor current ripple of different magnetic structures can be compared based on their equivalent circuit models listed in Fig. 4. In order to make a fair comparison, the total physical winding turns of the structure of Fig. 4 (a), (b), (c) are set to $3\beta N + 3N$.

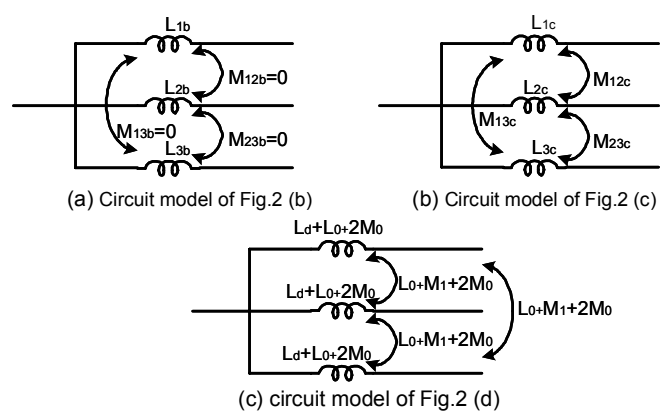

Fig. 4 The equivalent circuit modes of different magnetic structures

The inductance and mutual inductance of each structure is listed in table 1.

Table I The listed inductance and mutual inductance

Equivalent Circuit	Inductance L	Mutual Inductance M
Fig. 4 (a)	$(\beta+1)^2 N^2 C$	0
Fig. 4 (b)	$(\beta+1)^2 N^2 C\cdot\frac{2+2\alpha}{3+2\alpha}$	$-(\beta+1)^2 N^2 C\cdot\frac{1}{3+2\alpha}$
Fig. 4 (c)	$N^2 C\cdot\frac{6\alpha\beta^2-4\alpha\beta+2\alpha+2}{3+2\alpha}$	$N^2 C\cdot\frac{6\alpha\beta^2-4\alpha\beta-1}{3+2\alpha}$

There is a general set of equations for the above three structures:

$$\begin{cases} v_1 = L\dfrac{di_1}{dt} + M\dfrac{di_2}{dt} + M\dfrac{di_3}{dt} \\ v_2 = M\dfrac{di_1}{dt} + L\dfrac{di_2}{dt} + M\dfrac{di_3}{dt} \\ v_3 = M\dfrac{di_1}{dt} + M\dfrac{di_2}{dt} + L\dfrac{di_3}{dt} \end{cases} \tag{14}$$

v_1, v_2, v_3 are the voltages across the inductors and i_1, i_2, i_3 are the currents go though the inductors. Assuming the duty cycle $D < 1/3$, thus the resulting inductor current i_1 could be drawn as shown in Fig. 5. The inductor current ripple could be calculated as:

$$\Delta i_1 = \frac{V_{in}D}{LF_s}\frac{1+\lambda+\dfrac{2D}{D'}\lambda}{1+\lambda-\lambda^2} \tag{15}$$

Where V_{in} is the input voltage, F_s is the switching frequency and $\lambda = \dfrac{M}{L}$.

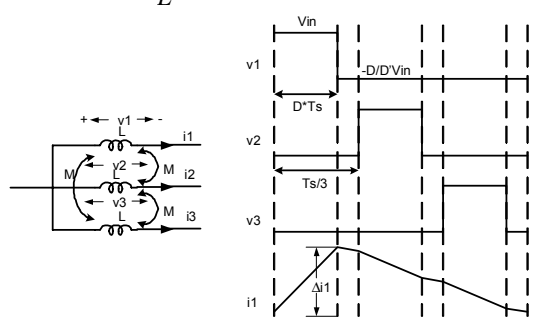

Fig. 5 Steady state switching waveforms for coupling inductors

The corresponding parameter λ for the three structures are:

$$\begin{aligned} \lambda_a &= 0 \\ \lambda_b &= M_b/L_b = -1/(2+2\alpha) \\ \lambda_c &= M_c/L_c = \frac{6\alpha\beta^2 - 4\alpha\beta - 1}{6\alpha\beta^2 - 4\alpha\beta + 2\alpha + 2} \end{aligned} \tag{16}$$

Substituting (16) to (15), the peak-to-peak value of the current ripple of three magnetic structures as plotted in Fig. 6. The ripple current Δi_a is normalized to one, and duty cycle is $D = 0.3$. The air gap factor α = 0.5. It is observed that Δi_b is always less than Δi_a from Fig. 6. However, for Δi_c, we have:

$$\begin{cases} \Delta i_c < \Delta i_b < \Delta i_{a,} \quad When\ \beta < \beta_1 \\ \Delta i_b < \Delta i_c < \Delta i_{a,} \quad When\ \beta_1 < \beta < \beta_2 \\ \Delta i_b < \Delta i_a < \Delta i_{c,} \quad When\ \beta > \beta_2 \end{cases} \tag{17}$$

When β is designed at β_0, the current ripple for the proposed magnetic structure has the minimum value and is much less than that of the other structures. Similar results as the above could be derived for 1/3<*D*<2/3 and 2/3<*D*<1.

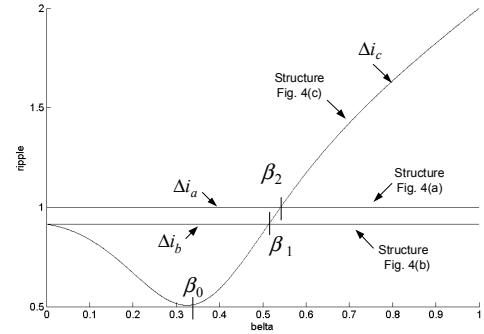

Fig. 6 Current ripple comparison among three structures

III. OPERATION PRINCIPLE AND ANALYSIS

The proposed converter topology was briefly introduced in section II. The detail operation principle and analysis is based on primary referred circuit.

A. Operation principle

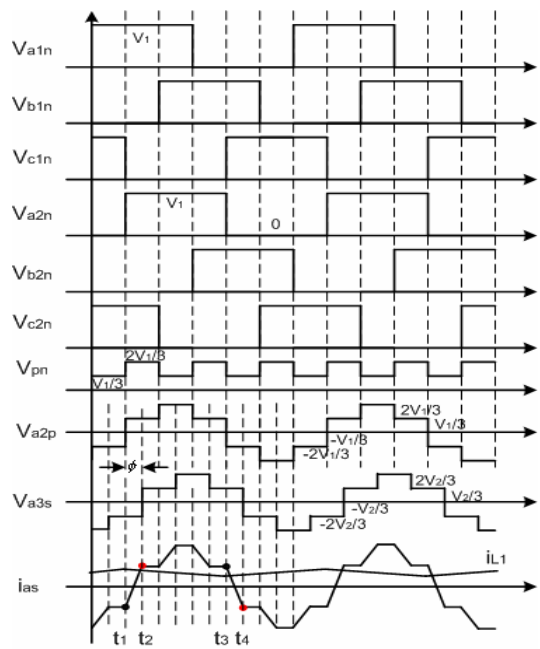

Fig. 7 Conceptual switching waveforms when V1=V2, D=0.5

Fig. 7 illustrates the key waveforms over a full switching cycle. The port I is operated under PWM control. The port II and port III are operated under PWM plus phase shift control. V_{a1n}, V_{b1n} and V_{c1n} are square waveforms generated by three- phase boost power stage of port I. V_{a2n}, V_{b2n} and V_{c2n} are square waveforms generated by TPDAB power stage. It should be noted that these six square waveforms are 60° apart from each other. In this case, smaller current ripple are expected for DC bus capacitor *C*1 since the ripple frequency is six times the switching frequency. The six-step line-to-neutral voltage waveform of the primary and secondary side of the transformer could be obtained in Fig. 7. There is a phase shift between these two voltage waveforms and the difference of the two voltages is applied on the

leakage inductance of the transformer to generate the inductor current i_{as}. There are twelve operation modes identified over a full switching cycle and transformer current under different modes was plotted accordingly. The output power could be derived in (18).

$$\begin{cases} P_o = \dfrac{V1 \cdot V2}{\omega L_s}\phi(\dfrac{2}{3} - \dfrac{\phi}{2\pi}), & When\, 0 \le \phi \le \dfrac{\pi}{3} \\ P_o = \dfrac{V1 \cdot V2}{\omega L_s}(\phi - \dfrac{\phi^2}{\pi} - \dfrac{\pi}{18}), & When\, \dfrac{\pi}{3} \le \phi \le \dfrac{2\pi}{3} \\ P_o = \dfrac{V1 \cdot V2}{\omega L_s}\phi(\dfrac{\phi}{3} - \dfrac{\phi^2}{2\pi} + \dfrac{\pi}{6}), & When\, \dfrac{2\pi}{3} \le \phi \le \pi \end{cases} \tag{18}$$

The TPDAB can be viewed as a multi-phase extension of ZVS dual half bridge circuit present in [11]. The soft-switching analysis is thereby derived similarly. As an example for phase A, the soft switching conditions for switches S_1, S_1', S_2 and S_2' are

$$\begin{cases} i_{as}(t_1) < i_{L1}(t_1) \\ \quad i_{as}(t_2) > 0 \\ i_{as}(t_3) > i_{L1}(t_3) \\ \quad i_{as}(t_2) < 0 \end{cases} \tag{19}$$

It could be easily found that all the switch conditions are satisfied when $V_1 = V_2$ shown in Fig. 7.

B. PWM plus phase shift control

Phase shift modulation plus PWM control are applied to bidirectional TPDAB converter to achieve the converter optimized operation including the minimization of current stress and maintaining soft switching conditions regardless the wide variation of dc operating voltage of UC.

Fig. 8 shows the transformer current and voltage of phase A when V1 < V2 where i_{as} exhibits large peak value and rms value. Moreover, $i_{as}(t_3) < i_{L1}(t_3)$ which means the switch S_2 does not satisfy soft switching. Fig. 9 shows the improved performance by adjusting duty cycle (increase D) to compensate the unbalance between LVS and HVS and make $V_1 = V_2$. The waveforms of Fig. 9 demonstrate lower peak value and rms value of i_{as} and in addition, all the switches now achieve soft switching again.

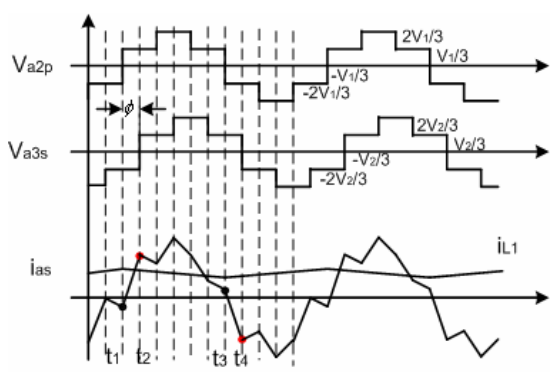

Fig. 8 The idealized operating waveforms with fixed D= 0.5 at V1<V2

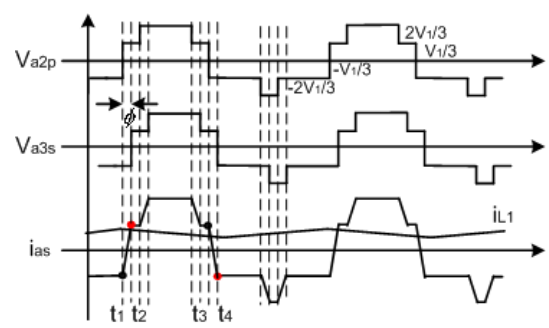

Fig. 9 The idealized operating waveforms with adjustable duty cycle at V1<V2

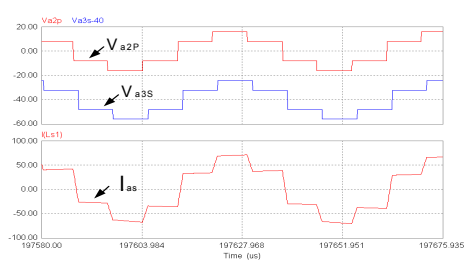

Fig. 10 Simulated operating waveforms with D=0.5 and V1=V2

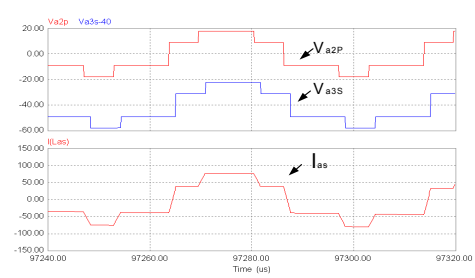

Fig. 12 Simulated operating waveforms with adjusted D and V1<V2

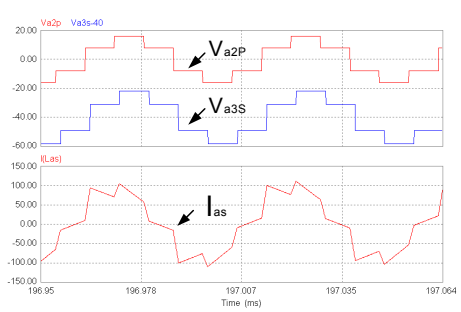

Fig. 11 Simulated operating waveforms with D=0.5 and V1<V2

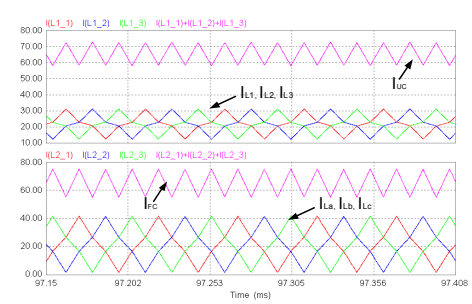

Fig. 13 Simulated output current waveforms of fuel cell and ultra-cap

The operation principle and phase shift plus PWM control was verified from Fig. 10 – 12 using circuit simulation. The parameters used in simulation are defined as below: $L_1 = L_2 = L_3 = 5\mu H$, Switching frequency $f_s = 20\,kHz$, transformer ratio = 1:1. The primary referred filter capacitors are $C_1 = C_2 = 0.02F$ and load resistance is $0.36\,ohm$. The primary referred three-phase leakage inductance $L_{as} = L_{bs} = L_{cs} = 0.3\,\mu H$.

In Fig. 10, $V_{in1} = V_{in2} = 12V$, $V1 = V2 = 24V$ and phase shift angle $\phi_a = \phi_b = \phi_c = 0.05\pi$. Fig. 11 shows the waveforms with output voltage $V2 = 27V$ and $\phi_a = \phi_b = \phi_c = 0.06\pi$. Duty cycle is kept at 0.5 and $V1$ is 24 V. The transformer current exhibits large peak value. Fig. 12 shows the waveforms with duty cycle $D = 0.55$ and phase shift is maintained at 0.05π . The transformer current becomes a flat six-step waveform again. The converter with phase shift plus duty cycle control can transfer the same amount of power with much less current stress and higher efficiency than the one with phase shift control only. Fig. 13 shows the current waveforms of interleaved coupled inductors connecting to fuel cell and ultra-cap with port I working in critical conduction mode.

TABLE 2. Component Stress Comparison at a specified operation condition

	DHB	TPDAB
Input Bridge		
No. of active devices	2	6
RMS current (A)/switch	S1: 70.6 S2: 266.5	S1: 24.6 S2: 85.5
Peak voltage (V)	32	32
Peak current (A)/switch	400	130
Output Bridge		
No. of active devices	2	6
RMS current (A)/switch	11.9	3.7
Peak voltage (V)	384	384
Peak current (A)/switch	18.5	6.2
Transformer specs.		
Transferring ratio	1:12	1:12
Peak primary volts (V)	16	21
Peak primary amps (A)/phase	220	90
RMS primary volts (V)	15.5	15
RMS primary amps (A)/phase	202	63.8
Peak secondary volts (V)	192	252
Peak secondary amps (A)/phase	18.3	7.5
RMS Secondary volts (V)	186	180
RMS secondary amps (A)/phase	16.8	5.3
Rating (kVA)/phase	3.5	0.95
Po/Rating	0.81	1
LVS Capacitor		
Voltage (V)	16	16
Peak current (A)	C11: 400, C12:200	100
RMS current (A)	C11: 70.6, C12:192.6	36.5
Rating (kVA)	C11: 1.2, C12: 3.08	0.584
HVS Capacitor		
Voltage (V)	192	192
Peak current (A)	25	1.66
RMS current (A)	9.35	1.1
Rating (kVA)	1.8	0.2

C. Component stress comparison

The proposed topology includes three-phase boost converter (port I) and TPDAB (port II and III). Since the advantages of three-phase boost converter have been addressed in many literatures, only TPDAB converter is compared here with its single-phase version dual half bridge (DHB) converter in Table 2. The comparison is based on a specified operation condition: Po=2850, Vin=16 V, Vo= 384 V and fs=20 kHz.

The table 2 shows the stress of each switching device of TPDAB converter is about one third of the single-phase topology. However, the total stress is about the same for both converters since the number of switching devices is increased three times in TPDAB converter. Considering the transformer utilization, the three-phase topology offers higher utilization factor (1.0) than the single-phase one (0.81). The current stress of input and output capacitors of three-phase topology is much lower than the single-phase circuit therefore smaller capacitor could be used for three-phase topology and power density will be improved.

IV. CONCLUSION

In this paper, a novel three-phase current source three-port dc-dc converter is proposed. A new design of three-phase inductor is presented with minimum current ripple. The power flow among three ports is analyzed as well as the soft switching conditions. The optimized operation of converter is achieved by adding controllable duty cycle to traditional phase shift control. The component stress of three-phase topology is compared with single-phase circuit at a specified operating condition. The simulation results verified the validity of the proposed circuit.

REFERENCES

[1] L. Solero, "Performance of a 10 kW power electronic interface for combined wind/PV isolated generating systems," in *Proc. IEEE PESC'96*, 1996, pp. 1027-1032.

[2] F. Caricchi, "Testing of a new DC-DC converter topology for integrated wind-photovoltaic generating systems," in *Proc. European Conf. Power Electronics and Applications*, 1993,pp.83-88.

[3] H. Matsuo, "Characteristics of the multiple-input dc-dc converter," in *Proc. IEEE PESC'93*, 1993, pp. 115-120.

[4] H. Matsuo, "Novel solar cell power supply system using the multiple-input dc-dc converter," in *Proc. INTELEC'98*, 1998, pp. 797-802.

[5] R. W.A.A.A. DeDoncker, D.M. Divan, M.H. Kheraluwala "A three-phase soft-switched high-power-density dc/dc converter for high-power applications," in *IEEE Trans. on Industry Applications,* vol.27, No.1, January/February, 1991, pp.63-73.

[6] P. Wong, P. Xu, B. Yang, F.C. Lee "Performance improvements of interleaving VRMs with coupling inductors," in *IEEE Trans. on Power Electronics,* vol.16, No.4, July, 2001, pp.499-507.

[7] W. Ren, Y.S. Lee"A two-channel interleaved boost converter with reduced core loss and copper loss," in *Proc. IEEE PESC'04*, 2004, pp. 1003-1009.

[8] J. Li, C. R. Sullivan, "Using coupled inductors to enhance transient performance of multi-phase buck converters," in *Proc. APEC'04*, 2004, pp. 1289-1293.

[9] C. Liu, A. Johnson, J. Lai "A novel three-phase high-power soft-switched DC/DC converter for low-voltage fuel cell applications," in *IEEE Trans. on Industry Applications,* vol.41, No.6, November/December, 2005, pp.1691-1697.

[10] D.C.Harnill "Lumped equivalcnt cireuils of magnetic components: The gyrator-capacitor approach," in *IEEE Trans. On Power Electronics,* vol.8, No.2, November/December, 2005, pp.97-103.

[11] Fang Z. Peng, Hui Li, Gui-jia Su, J. Lawler, "A New ZVS Bi-directional dc-dc Converter for Fuel Cell and Battery Applications," *IEEE Transaction on Power Electronics*, Vol. 19, No.1, Jan 2004, pp.54-65.

[12] D. Xu, C. Zhao, H. Fan "A PWM plus phase-shift control bidirectional dc-dc converter," in *IEEE Trans. on Power Electronics,* vol.19, No.3, May, 2004, pp.666-675.